THE JOURNAL OF BIOLOGICAL CHEMISTRY VOL. 287, NO. 12, pp. 9072–9080, March 16, 2012

Solution Structure of Homology Region (HR) Domain of Type II Secretion System*[S]

Received for publication, September 2, 2011, and in revised form, January 13, 2012 Published, JBC Papers in Press, January 17, 2012, DOI 10.1074/jbc.M111.300624

Shuang Gu[‡], Geoff Kelly[§], Xiaohui Wang[¶], Tom Frenkiel[§], Vladimir E. Shevchik[¶1], and Richard W. Pickersgill[‡2]

From the [‡]School of Biological and Chemical Sciences, Queen Mary University of London, London E1 4NS, United Kingdom, [§]MRC Biomedical NMR Centre, National Institute for Medical Research, The Ridgeway, Mill Hill, London NW7 1AA, United Kingdom, and the [¶]Université de Lyon, F-69003, Université Lyon 1, Lyon, F-69622, INSA-Lyon, Villeurbanne F-69621, CNRS, UMR5240, Microbiologie Adaptation et Pathogénie, Lyon, F-69622, France

Background: The HR domain is essential for the function of the T2SS.
Results: HR domain has similar structure to PilP of the T4PS and interacts with secretin.
Conclusion: The evolutionary link between T2SS and T4PS extends to proteins of the inner membrane subcomplex.
Significance: This work is crucial to understanding how this machine works and how it may be stopped.

The type II secretion system of Gram-negative bacteria is important for bacterial pathogenesis and survival; it is composed of 12 mostly multimeric core proteins, which build a sophisticated secretion machine spanning both bacterial membranes. OutC is the core component of the inner membrane subcomplex thought to be involved in both recognition of substrate and interaction with the outer membrane secretin OutD. Here, we report the solution structure of the HR domain of OutC and explore its interaction with the secretin. The HR domain adopts a β-sandwich-like fold consisting of two β-sheets each composed of three anti-parallel β-strands. This structure is strikingly similar to the periplasmic region of PilP, an inner membrane lipoprotein from the type IV pilus system highlighting the common evolutionary origin of these two systems and showing that all the core components of the type II secretion system have a structural or sequence ortholog within the type IV pili system. The HR domain is shown to interact with the N0 domain of the secretin. The importance of this interaction is explored in the context of the functional secretion system.

Gram-negative bacteria have evolved multiple sophisticated machines to transport selected proteins across the two bacterial membranes. The type II secretion system (T2SS)[3] is specifically used to secrete folded proteins such as lytic enzymes and toxins from the periplasm to the external medium or to host tissue (1, 2). This system is shared by many bacteria pathogenic for human, animals, and plants where it plays a pivotal role in pathogenesis. The T2S machinery is composed of 12 to 15 components with generic names GspA to GspO. The T2SS components of the phytopatogen bacteria *Dickeya dadantii* (formerly *Erwinia chrysanthemi*) are named Out. Most of these proteins are multimeric and build together a sophisticated machine spanning both bacterial membranes. The machine can be divided into three subassemblies. The secretin GspD (Gsp is the nomenclature for the enterotoxigenic *Escherichia coli* and Out for *D. dadantii* proteins) forms large gated channels in the outer membrane through which the proteins are secreted (3, 4). Five pseudopilins (GspG to GspK) are processed by the prepilin peptidase/methylase GspO and form a short pilus not exceeding the periplasm, which could push proteins to be secreted through the pore formed by the secretin. GspC, GspL, GspM, and GspF are thought to form a subcomplex in the inner membrane (5). An ATPase, GspE is associated with this subcomplex and provides energy to the secretion process probably by assuring assembly of the pseudopilus (6). However, the exact role of individual components and the molecular organization of the T2S machinery have remained elusive.

Phylogenetic analyses suggested that the T2SS is ancestrally related to the type IV pili system (T4PS) and share several homologous core elements (7). The current models of T2S also suggest its functional similarity with T4P system, notably, that short pseudopilus assembled in the periplasm push the protein across the pore formed by the secretin. Because the inner membrane components of T2SS and T4P, GspL/M/C, and PilM/N/O/P, respectively, do not share any sequence similarity, they have been assumed to execute functions specific for each of these systems (1, 8). However, recent structural analysis

* This work was supported by the Biology and Biotechnology Sciences Research Council (U.K), Higher Education Funding Council for England, and Queen Mary University of London.

The atomic coordinates and structure factors (code 2LNV) have been deposited in the Protein Data Bank, Research Collaboratory for Structural Bioinformatics, Rutgers University, New Brunswick, NJ (http://www.rcsb.org/).

NMR spectra and assignments have been deposited in the BioMagResBank under accession no. 18181.

[S] This article contains supplemental Tables S1 and S2 and Figs. S1–S4.

[1] Supported by a grant from French ANR-2010-BLANC-1531 SecPath program. To whom correspondence may be addressed: Université de Lyon, F-69003, Université Lyon 1, Lyon, F-69622, INSA-Lyon, Villeurbanne F-69621, CNRS, UMR5240, Microbiologie Adaptation et Pathogénie, Lyon F-69622, France. Tel.: 04-72-44-58-27; Fax: 04-72-43-15-84; E-mail: vladimir.shevchik@insa-lyon.fr.

[2] To whom correspondence may be addressed: School of Biological and Chemical Sciences, Queen Mary University of London, London E1 4NS, UK. Tel.: 44-0-20-7882-8444; Fax: 44-0-20-7882-7732; E-mail: r.w.pickersgill@qmul.ac.uk.

[3] The abbreviations used are: T2SS, type II secretion system; T4PS, type IV pili system; HR, homology region; r.m.s.d., root mean square deviation.

revealed that the periplasmic domains of GspL and PilN on one side and GspM and PilO on the other adopt the same ferredoxin-like fold and hence could play similar functions within T2S and T4P systems, respectively (9–11). Moreover, the cytoplasmic region of GspL adopts the actin-like fold of PilN (12). Therefore, GspC is yet the sole T2SS core component that has not a sequence or structural ortholog within the T4PS. GspC is a bitopic inner membrane protein. The single trans-membrane segment drives dimerization of the protein (13). The periplasmic region possesses a so-called homology region (HR) and, in most known GspCs, including OutC, a PDZ domain (see Fig. 1*A*). The PDZ domain is involved in secretion specificity but is not an essential module because in certain GspCs, it is absent or replaced by a coiled-coil domain (14). The exact function of HR is unknown; however, it was shown to interact *in vitro* with the N-terminal region of the secretin GspD and especially with the N0 domain (15, 16).

Secretins constitute the outer membrane pore necessary for translocation of macromolecules. Beyond the T2SS system, secretins are also involved in T4P, T3SS and filamentous phage release (17). Secretins consist of two main regions, a variable N-terminal periplasmic region and a conserved pore-forming C-domain, also named the secretin domain. The N-terminal region has a modular structure and in secretins from different systems possesses a variable number of N0, N1/N2, and N3 domains (18, 19). A schematic of the domain organization of OutD the cognate secretin for OutC is also shown in Fig. 1*A*. This N-terminal region is thought to assure specific functions within each of the export pathways. Notably, it interacts with the inner membrane components of secretion systems and with the proteins to be exported (4, 19, 20).

In this work, we report determination of the solution structure of the homology region domain of OutC and investigate its interaction with the secretin OutD from the plant pathogenic bacteria *Dickeya dadantii* both *in vitro* and *in vivo*. This study reveals a striking structural similarity between the HR domain and the periplasmic domain of PilP from the T4PS, revealing that these important components of the inner membrane subcomplexes evolved from a common ancestor; this strengthens the view that these molecular machines have a common evolutionary origin. We also show that β1 of the HR domain interacts with the N0 domain *in vitro* and explore the importance of the interactions involved *in vivo*.

EXPERIMENTAL PROCEDURES

Protein Expression, Purification, and Analysis—The HRF3 fragment was discovered using limited proteolysis of the protein produced using the pGX-oC-HR construct (supplemental Table S1). Sequencing grade trypsin was used. The protein sample was bound to a C5 reverse-phase HPLC column in the presence of 1% formic acid solution and eluted using an acetonitrile gradient. Three fractions from the HPLC column were characterized by mass spectroscopy, HRF1, -2, and -3; HRF3 was the shortest of these nested fragments and was therefore selected for further study. N0, N1, and N1-N2 domains of OutD were produced in *E. coli* and purified by nickel-affinity chromatography as described previously (13).

The HRF3 DNA was amplified from HR construct (pGX-oC-HR) and cloned into the pET14b expression vector (strains and primers used are detailed in supplemental Tables S1 and S2). The expression vector was transformed into competent BL21 (DE3) *E. coli* cells. Following bacterial growth and induction the protein was loaded onto a 5-ml His Trap HP column. After washing, Thrombin (GE Healthcare) was used to release the His tag cleaved HRF3 from the column. HRF3 was then passed through a Superdex75 column (GE Healthcare) column. The fragment eluted at a volume consistent with HRF3 being a subunit in solution. This was confirmed by dynamic light scattering. For NMR spectroscopy, uniformly ^{15}N- and ^{13}C-labeled proteins were produced by growing cell cultures in M9 minimal medium that contained 1 g/liter ^{15}N-ammonium chloride and 2 g/liter ^{13}C-D-glucose (Cambridge Isotope Laboratories, Inc.) as the sources of nitrogen and carbon, respectively.

NMR Spectroscopy—NMR spectra were acquired at 15 °C using Bruker Avance 700 and 600 MHz spectrometers equipped with CryoProbes. NMR samples had a typical concentration of 0.3–0.7 mM in 20 mM Tris, pH7.0, and 10% D_2O. 150 mM NaCl was included in the cross-titration studies. Fast chemical shift-based structure calculations were used initially employing CS-Rosetta (21, 22). All spectra were processed using NMRPipe/NMRDraw (23) and analyzed using XEASY (24). HNCA, HN(CO)CA, HNCO, HNCACB, and CBCA(CO)NH experiments were employed to obtain sequence-specific ^{1}HN, ^{15}N, $^{13}C\alpha$, $^{13}C\beta$, and $^{13}C'$ backbone assignments. Side chain aliphatic proton and carbon assignments were achieved by a combination of three-dimensional ^{15}N-edited total correlation spectroscopy- and NOESY-heteronuclear single-quantum correlation spectroscopy (25). Secondary structure elements were determined from a combination of ^{1}HN, ^{15}N, $^{13}C\alpha$, $^{13}C\beta$, and $^{13}C'$ secondary chemical shifts using TALOS+ (26, 27) as well as from identification of interstrand NOE contacts. Hydrogen bonds were measured by direct trans-hydrogen bond (N-H–O=C) scalar coupling (28). Structure calculation used ARIA (version 1.2) (29) and input NOE data from three-dimensional ^{15}N-edited NOESY-HSQC, ^{13}C-edited NOESY-HSQC (all acquired with a mixing time of 100 ms), 76 φ and ψ torsion angles were derived from TALOS and residual dipolar coupling measurements. The standard ARIA protocol was used with nine iterations and 100 structures generated per iteration. In the final iteration, 30 structures with the lowest energy were used for water refinement and 20 structures with the lowest energy were selected as representatives of OutC-HRF3 structure.

In Vivo Analysis of Mutant OutC and OutD Variants—To test the functionality of OutC and OutD variants carrying site-specific substitutions, complementation assays were used with *D. dadantii* A3556 Δ*outC* and A3558 Δ*outD* strains. Bacteria carrying an appropriate pTdB plasmid with a mutant allele of either *outC*, or *outD*, or *outC-outD* were grown in Luria-Bertani medium supplemented with sodium galacturonate at 1 g·liter^{-1} at 30 °C aerobically at 150 rpm to steady-state; then, culture supernatant and cells were separated by centrifugation and analyzed by immunoblotting with PelD and PelI antibodies as described previously (13). Abundance of the OutC and OutD mutant variants in the cells was assessed by immunoblotting

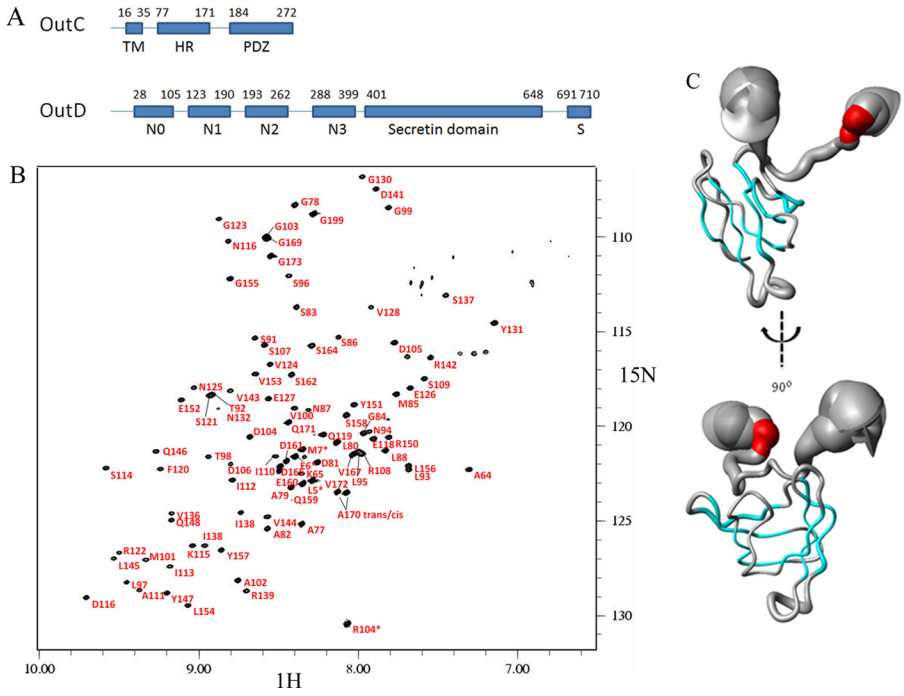

FIGURE 1. **Tertiary structure of the HR domain of OutC.** *A*, schematic representation of the domain organization of inner membrane subcomplex component OutC and secretin OutD. *B*, assignment of the ^{1}H-^{15}N HSQC spectra for the HR domain. *C*, sausage representation of the best 20 calculated OutC-HRF3 structures. The secondary structure is shown in color: α-helical residues are in *red*, and the β-sheet is in *cyan*. The diameter of the sausage reflects the dynamics of the protein in solution, which is plotted according to the residue α-carbon T2 relaxation profile.

with OutC and OutD antibodies. For *in vivo* disulfide bonding analysis, *D. dadantii* cells carrying appropriate plasmids with mutant *outC* and/or *outD* genes were grown as above. Cells were washed in TBS (50 mM Tris-HCl, pH 7.5, 100 mM NaCl), and remaining free thiol groups were blocked with 20 mM iodoacetamide in TBS at 25 °C for 30 min. The cells were then pelleted, resuspended in Laemmli sample buffer without 2-mercaptoethanol and boiled for 10 min, and the extent of disulfide bonding was assessed by SDS-PAGE, followed by immunoblotting with anti-OutC and anti-OutD antibodies.

RESULTS

Identification of Folded Homology Region Domain (OutC-HR)—OutC comprises a short cytoplasmic sequence, a transmembrane helix, and two periplasmic regions: the homology region and a PDZ domain (Fig. 1*A*). The HR region is so named because a similar sequence is found in all GspC proteins. Examination of the ^{1}H-^{15}N HSQC spectrum of the periplasmic region of OutC (residues 60 to 272) reveals that in addition to the PDZ domain, there is also another folded domain. Limited proteolysis of this OutC derivative gave three bands (HRF1, HRF2, and HRF3) on both SDS-PAGE and native gel (supplemental Fig. S1). The native gel was used to assess the solubility of the proteolytic fragments as insoluble protein tends to aggregate and not enter the gel. The precise identities of the fragments were established by mass spectroscopy (supplemental Fig. S2) and confirmed by N-terminal sequencing. The smallest fragment (HRF3), corresponding to residues 77 to 172, was produced recombinantly by sub-cloning the appropriate part of the *outC* gene. The HRF3 protein produced in this way was both soluble and stable and was used for these studies. The ^{1}H-^{15}N HSQC spectrum of HRF3 was well dispersed and overlaid well with the previously measured spectrum for the entire periplasmic region of OutC, confirming that HRF3 comprises an independently folded domain (supplemental Fig. S3).

Solution Structure of Homology Region Domain of OutC—NMR relaxation measurements revealed that the structured region of HRF3 comprised 67 residues (residues 91 to 157), and we refer to this domain as the homology region (HR) domain. A nearly complete sequence-specific NMR signal assignment was achieved using a combination of three-dimensional triple resonance experiments using ^{15}N,^{13}C-labeled OutC-HR, and three-dimensional NOSEY-HSQC, TOCSY-HSQC using ^{15}N-labeled protein (Fig. 1*B*). The 1954 experimental NOE distance restraints were obtained using isotope-edited NOESY spectra, and 76 φ and ψ torsion angle restraints were derived from secondary chemical shift analysis using the TALOS algorithm. Twenty eight hydrogen bonds were measured experimentally. The structure of the folded domain was determined with high precision as judged from the overall root mean square deviation (r.m.s.d.) of 0.46 and 1.26 Å for the backbone and heavy atoms, respectively (Table 1) for the pairwise r.m.s.d. for the family of 20 representative structures. It is significant that even the loop regions connecting the anti-parallel β-strands are well determined in this structure (Fig. 1*C*). It is interesting to note that the structure predicted by CS-ROSETTA, using only the chemical shift data, was very close to that determined using conventional methods.

The architecture of the central 67 residues is β-sandwich-like comprising two three-stranded (up-down-up) anti-parallel β-sheets with short hairpin loops connecting adjacent β-strands within the two sheets and a longer loop between the two sheets (Fig. 2, *A*–*C*). The angle between the strands

TABLE 1
NMR refinement statistics for the HR domain (OutC-HRF3)

NMR distance and dihedral constraints	
Distance constraints	
Total NOE	1954
Intra-residue	652
Inter-residue	
Sequential ($\|i-j\|=1$)	381
Medium range ($\|i-j\| \geq 2 \leq 4$)	170
Long range ($\|i-j\| \geq 5$)	751
Hydrogen bonds (experimental measured)	28
Hydrogen bonds(observed in >50% of structures)	64
Total dihedral angle restraints (TALOS)	76
φ	38
ψ	38
Structure statistics	
Violations (mean ± S.D.)	
Distance constraints (>0.5) (Å)	0
Dihedral angle constraints (>5) (°)	0
Deviations from idealized geometry	
Bond lengths (Å)	0.005 ± 0.0001
Bond angles (°)	0.671 ± 0.011
Impropers (°)	0.748 ± 0.024
Average pairwise r.m.s.d. (Å)[a]	
Backbone	0.46 ± 0.11
Heavy	1.26 ± 0.20
R.m.s.d. from the mean structure (Å)[a]	0.33 ± 0.07
Residues in allowed regions[b]	98.3%
Residues in disallowed regions	1.7%

[a] Pairwise r.m.s.d. and r.m.s.d. from the mean structure were calculated among the 20 lowest energy structures from 50 refined structures (amino acid residues 91 to 157).
[b] Structure quality was analyzed with MolProbability over structured regions (amino acid residues 91–157). One residue in a tight β-turn between β5 and β6 (Pro^{140}) is in a disallowed region.

in the two β-sheets is ~45°. In several members of the family of structures, there is a fourth β-strand in the second β-sheet. This strand is more dynamic in solution than the other six β-strands, which are present in each of the 20 structures. The first β-strand is involved in interaction with the N0 domain of OutD and is illustrated in Fig. 2*D* (see also results below). Aliphatic residues, mostly leucines, from the internal surface of the β-sheets form the hydrophobic core of the HR domain (Fig. 2*E*). To both the N- and C- terminal ends of the β-sandwich, there are ~20 residues that are less regular in structure.

HR Domain Is Structurally Similar to PilP—A Dali database search revealed that the HR domain is similar to the periplasmic domain of PilP, an inner membrane core component of the T4PS of *Neisseria meningitidis* (Protein Data Bank code 2IVW) (30). The Z score is 3.7, and root mean square deviation is 6.8 Å for 64 equivalent α-carbon atoms. The HR domain has the same β-strand topology and common β-sandwich type fold as PilP (Fig. 2, *A–C*). In some of the HR family of structures, the conserved β4 strand of PilP is frequently not formed revealing greater structural flexibility in this part of the HR domain. To aid comparison with PilP, and in light of this flexible "β4" region, we use the same β-strand numbering for HR as used previously for PilP. Sequence alignment of PilP homologs from various T4PS indicates that strand β4 together with short neighboring loops L4 and L5 constitute a more conserved

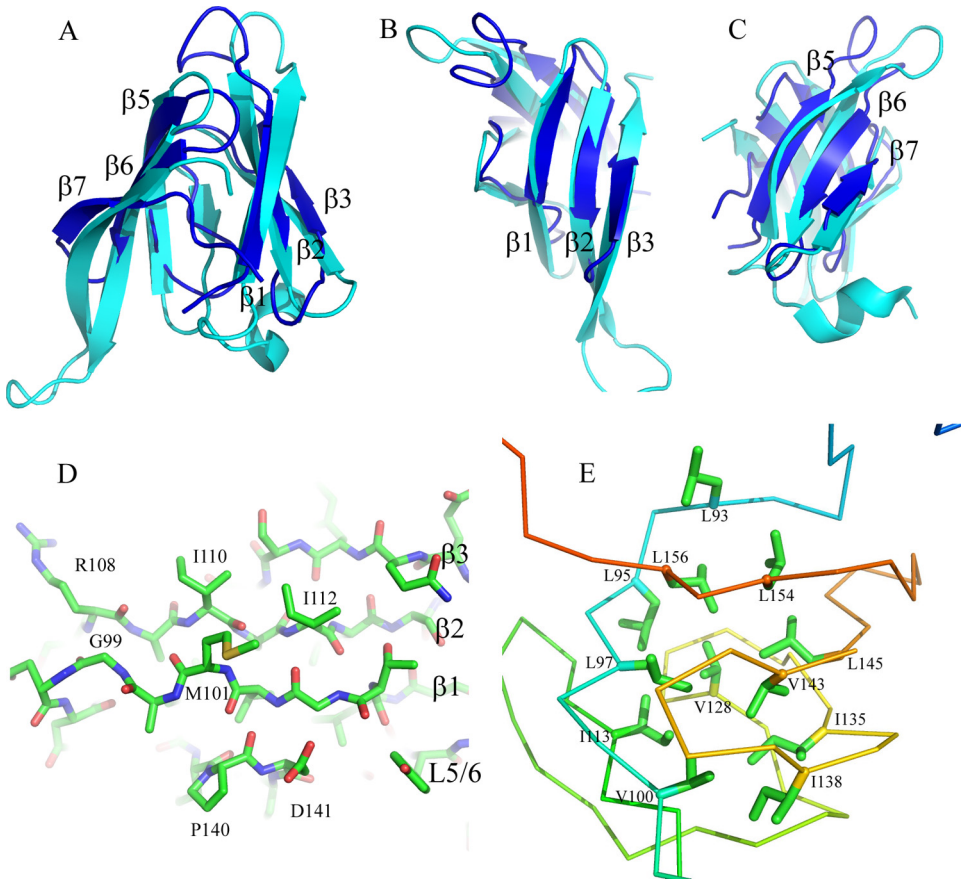

FIGURE 2. **HR domain structure compared with PilP.** *A*, schematic representation of the structure of the HR domain (*blue*) superimposed on PilP (*cyan*). The β-strands are labeled according to PilP numbering. *B* and *C* look down onto the first and second sheet of the HR domain, respectively. *D*, the first β-sheet in stick representation, highlighting β1, which is important in the interaction of HR with OutD-N0 (see Fig. 5). *E*, hydrophobic residues forming the core of the HR domain in stick representation with backbone displayed as a ribbon.

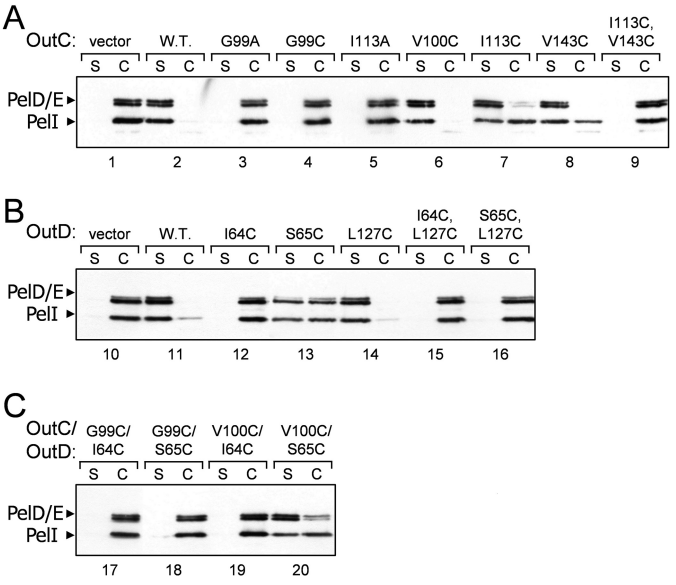

FIGURE 3. **Functional analysis of OutC and OutD point mutants.** The secretion activity of OutC and OutD mutants (indicated on *top* of gels) was estimated in a complementation assays with *D. dadantii* strains A3656 Δ*outC* (*A* and *C*) and A3658 Δ*outD* (*B*). Bacteria carrying a plasmid with mutant alleles of either *outC* (*A*), or *outD* (*B*), or *outC* and *outD* (*C*) were grown to steady-state; then, culture supernatant (*S*) and cells (*C*) were separated and analyzed by immunoblotting with PelD and PelI antibodies. The amount of secreted proteins (PelD, PelE, and PelI) in culture supernatant reflects secretion efficiency. The abundance of the corresponding OutC and OutD variants is shown on Fig. 4.

region than the corresponding region of the HR sequence (supplemental Fig. S4).

Several Conserved Residues Form Hydrophobic Core of HR—The two β-sheets composing the HR domain seem largely independent and are connected together through several hydrophobic interactions, including the side chains of well conserved Leu^{93}, Leu^{97}, Ile^{113}, Val^{143}, Leu^{154}, and Leu^{156} and semiconserved Leu/Ile^{145}, $Ile/Leu/Val^{135}$, and Ile/Val^{138} (Fig. 2*E* and supplemental Fig. S4). Most of these residues are also conserved in the PilP periplasmic domain highlighting their structural importance. Ile^{113} and Val^{143} contribute to the hydrophobic packing between the two sheets. The proximity of Ile^{113} and Val^{143} was assessed *in vivo* by site-directed mutagenesis and cysteine mediated cross-linking analysis. Substitution of one of these residues with cysteine did not affect notably the secretion in *D. dadantii*, whereas substitution with alanine impaired it (Fig. 3*A*, *lanes 5*, *7*, and *8*), indicating that in contrast to cysteine, alanine is not able to replace these hydrophobic side chains. A non-reducing gel revealed that $OutC^{I113C}$ and $OutC^{V143C}$ remained mostly as a non-cross-linked subunit (Fig. 4*A*, *lanes 4* and *5*), implying that the corresponding side chains are poorly accessible for intermolecular disulfide formation. Double I113C/V143C substitution fully prevented secretion (Fig. 3, *lane 9*) and provoked an efficient intramolecular disulfide bond within OutC (Fig. 4*A*, *lane 6*). Indeed, on non-reducing gel, $OutC^{I113C/V143C}$ migrated slightly faster indicative of its more compact shape. These mutational analyses are consistent with the solution structure determined for the HR domain.

OutC-HR Domain Interacts with OutD-N0 Domain—Previous NMR studies had demonstrated that the periplasmic part of OutC (residues 60 to 172 corresponding to the periplasmic region of OutC with the PDZ domain deleted) interacted with the N-terminal domains (N0, N1, N2, N3) of the secretin OutD (16). When unlabeled N0 domain (residues 28 to 112) was titrated into ^{15}N-labeled HR domain (residues 77 to 172), the peaks loosing intensity on the ^{1}H-^{15}N-HSQC spectra were those seen to lose intensity when the N-terminal domains of OutD were titrated into $OutC^{60-272}$ (supplemental Fig. S3). This confirms that it is the HR domain that is interacting with the periplasmic domains of OutD. However, shifts were not observed when the domain pair N1-N2 (residues 116 to 285) was titrated into the labeled HR domain. These data reveal that the N0 domain and not the N1-N2 domains interact with the HR domain. The major peak shifts on the ^{1}H-^{15}N-HSQC spectra when N0 was added involved β1 of the HR domain (Fig. 5*A*).

Non-linear sampling methods were then used to collect data from ^{13}C,^{15}N-labeled N0 domain allowing the assignment of 65 of the 80 residues. The backbone chemical shifts confirmed that the secondary structure of *D. dadantii* N0 was the same as that of *E. coli* N0, and a reasonable model of the *D. dadantii* N0 domain could therefore be built using the *E. coli* domain as a template. The chemical shifts observed when unlabeled HR domain was added could now be mapped to the surface of the N0 domain. The chemical shifts observed reveal that residues on strands β1, β2, and β3 of the HR domain interact with N0 with residues on β1 most affected (Fig. 5). Residues on β1 and α2 of the N0 domain were the most affected, but the shifts were relatively small. Small shifts were seen for residues: Thr^{63}, Ile^{64}, Ser^{65}, Phe^{79}, Ser^{83}, and Val^{84}. A model of the HR·N0 complex was produced using HADDOCK (31) and is shown in Fig. 5*B*. The model brings β1 of HR and β3 of N0 together such that they could form a continuous anti-parallel β-sheet across both domains HR and N0. It is important to note that this is only a model of the interaction and the position and conformation of interfacial residues has not been defined experimentally. Met^{101} appears to be an important hydrophobic residue at the interface with the more remote Asp^{141} also showing large chemical shifts. The interaction between the *D. dadantii* HR and N0 domains is weak, but it does persist in the presence of 150 mM sodium chloride. The biological relevance of the interaction is assessed in the next section.

Assessment of HR Residues Involved in HR-N0 Interaction in Vivo—NMR cross-titration studies indicated that the HR-N0 interface includes the first β-strand of HR, notably Gly^{99}, Val^{100}, and Met^{101} (Figs. 2*D* and 5). Moreover, the latter residue and Asp^{141} showed large chemical shifts on binding. To explore the functional importance of these residues, they were substituted with alanine and cysteine and assessed in secretion assays (Fig. 3*A*). The D141A substitution was fully functional, indicating that this conserved residue (supplemental Fig. S4) is not crucial for the interaction with N0 and therefore has some other functional significance. Similarly, substitution of Val^{100} with cysteine did not affect the secretion (Fig. 3*A*, *lane 6*), implying that cysteine can be accommodated in place of the valine without perturbation of the β-sandwich architecture. In contrast, Gly^{99} and Met^{101} could not be substituted without total loss of secretion function (Fig. 3*A*), indicating their crucial structural and functional roles, respectively. Substitution of Met^{101} with alanine would lead to a loss of hydrophobic surface affecting

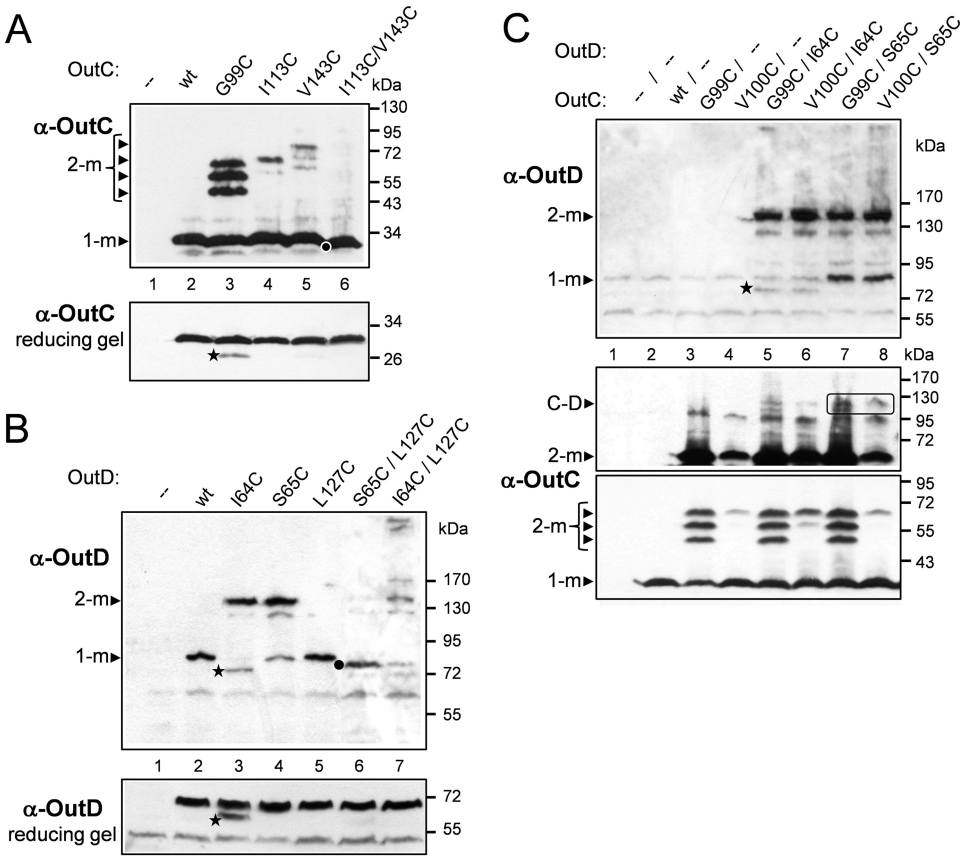

FIGURE 4. **Disulfide cross-linking analysis of OutC and OutD interactions within the functional T2SS.** *A*, disulfide cross-linking analysis of the HR domain of OutC. The G99C substitution provokes efficient homodimerization of OutC, whereas I113C or V143C single substitutions do not. Double substitution I113C/V143C leads to an intramolecular disulfide within OutC. *B*, disulfide cross-linking analysis of N0-N1 interaction sites in OutD. I64C and S65C single substitutions provoke efficient homodimerization of OutD, whereas L127C substitution does not. Double substitution S65C/L127C causes an intramolecular disulfide between N0 and N1 domains of OutD, whereas I64C/L127C does not. *C*, disulfide bonding analysis of HR-N0 interacting site. Combination of G99C and V100C substitutions in OutC with I64C and S65C substitutions in OutD does not provoke an efficient cross-linking between OutC and OutD. Some amounts of putative OutC·OutD complex are surrounded. *D. dadantii* strains A3556 Δ*outC* (*A* and *C*) and A3558 Δ*outD* (*B*) carrying a plasmid with mutant alleles of either *outC* (*A*), or *outD* (*B*), or *outC* and *outD* (*C*) (cysteine substitutions indicated on *top*) were grown aerobically to steady-state. Remaining free thiol groups were blocked with iodoacetamide, and the extent of disulfide bonding was assessed by SDS-PAGE under non-reducing conditions followed by immunoblotting with anti-OutC and anti-OutD antibodies. The same samples but treated with 2-mercaptoethanol were used to estimate abundance of the corresponding OutC and OutD variants (reducing gel). In *C*, the *middle panel* was overexposed in comparison with the *lower panel* to show high molecular mass species. Positions of monomers (*1-m*) and dimers (*2-m*) and putative OutC·OutD complex (*C* and *D*) are indicated by *arrowheads*. *Stars* indicate degradative products of OutCG99C and OutDI64C variants. *Dots* indicate OutCI113C/V143C and OutDS65C/L127C variants that migrate slightly faster than the corresponding wild-type monomers, indicating formation of an intramolecular disulfide bond.

interactions involving the HR-β1 interface. Gly^{99} is the most conserved residue among HR and PilP (supplemental Fig. S4). It is located in the center of β1 strand and introduces a bend to facilitate formation of β-bulge. Contrary to the other single cysteine substitutions in HR, $OutC^{G99C}$ formed dimers very efficiently (Fig. 4*A*, compare *lane 3* with *lanes 4* and *5*, Fig. 4*C*, *lower panel*, compare *lane 3* with *4*), suggesting that in the assembled secretion system, neighboring HR domains might interact via the first β-strand.

In Vivo Assessment of HR-N0 and N0-N1 Interactions—To probe *in vivo* proximity of β1 of HR with β3 of N0 domain, several residues located on these two β-strands were simultaneously substituted with cysteine in an attempt to isolate a disulfide bridged OutC and OutD pair. Single cysteine substitution of Ile^{64} and Ser^{65} on β3 of N0 provoked homodimerization of the mutant OutD (Fig. 4*B*, *lanes 3* and *4*), suggesting that in the functional T2SS, neighboring N0 domains could interact together through the β3 strand. When these mutations in OutD were combined pairwise with G99C and V100C substitutions in OutC, only low amounts of OutC·OutD complex was observed with $OutC^{G99C}$/$OutD^{S65C}$ couple (Fig. 4*C*, *middle panel*, *lane 7*). Perhaps an optimal arrangement of residues or the distance adequate for disulfide formation was not achieved.

We further probed by cysteine cross-linking analysis the crystal interface observed previously between the β3 of N0 and β6 of N1. This interface includes several pairs of proximal residues, notably Ser^{65} and Leu^{127}, on β3 and β6, respectively. Single L127C substitution behaved as the wild-type protein, was fully functional and was monomeric (Fig. 3*B*, *lane 14*, and Fig. 4*B*, *lane 5*). However, double S65C/L127C substitution became non functional (Fig. 3*B*, lane 16) and formed an intramolecular disulfide bond because it migrated faster than monomeric OutD (Fig. 4*B*, compare *lanes 5* and *6*). In contrast, L127C combined with I64C did not generate such an intramolecular cysteine bonding (Fig. 4*B*, *lane 7*). These data are compatible with mutual arrangement of the assessed residues within the N0/N1 crystal interface, where Ile^{64} is buried, whereas Ser^{65} and Leu^{127} are exposed to the interface. These

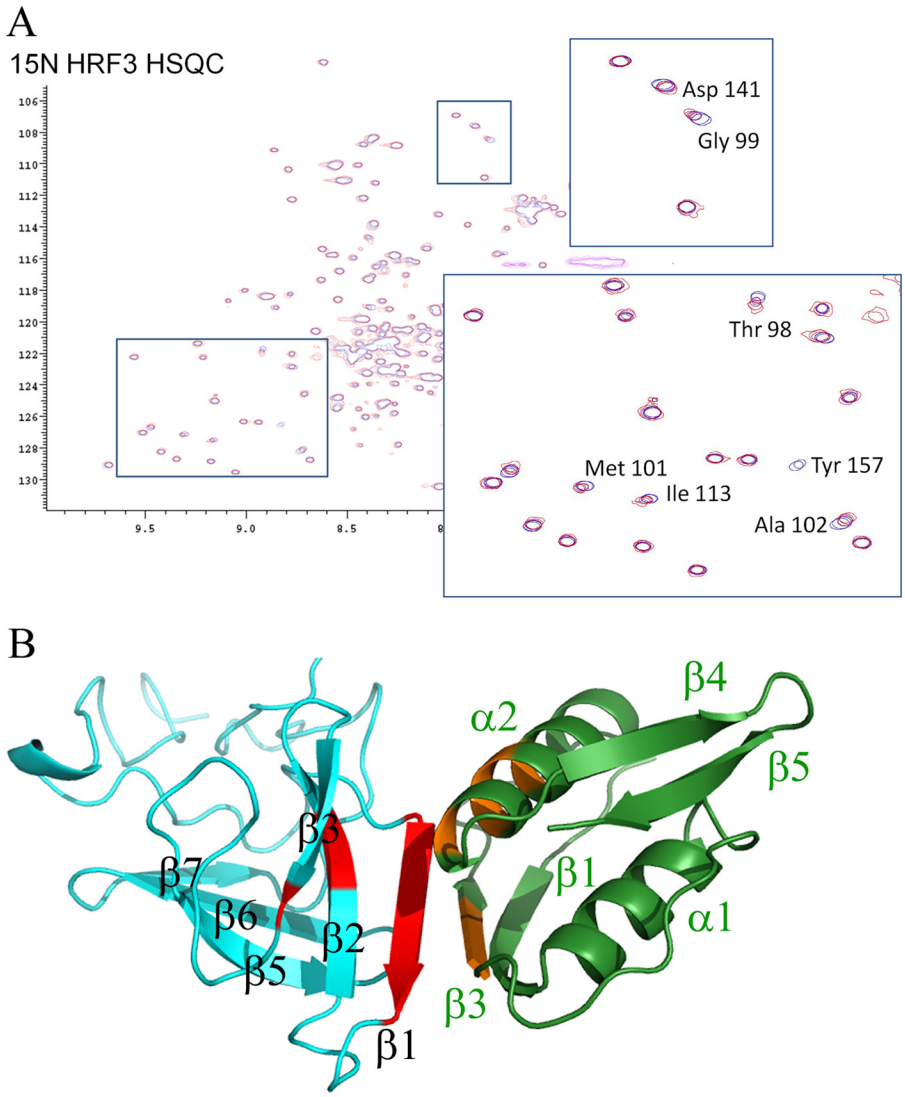

FIGURE 5. **HADDOCK model of the OutC-HR·OutD-N0 complex in schematic representation.** *A*, chemical shifts measured for the ^{15}N-HR domain when unlabeled N0 is added. *B*, the HR domain is on the *left* in *cyan*, and the N0 domain on the *right* in *green*. Chemical shifts are mapped onto the structures of HR domain in *red* and onto the N0 domain in *orange*, respectively. β1 of the HR domain interacts with β3 and α2 of N0. The peaks shifted on HRF3 are Thr^{98}, Gly^{99}, Val^{200}, Met^{101}, Ala^{102}, Ile^{112}, Ile^{113}, Phe^{120}, Asp^{141}, and Tyr^{88}. On N0, the peaks shifted are Thr^{63}, Ile^{64}, Ser^{65}, Phe^{79}, Ser^{83}, and Val^{84}. This is a modeled structure not an experimentally derived structure.

results reveal that β3 of the N0 domain can interact as well with an adjacent N0 domain (via β3-β3 strand interaction) as with N1 domain (via β3-β6 strand interaction) (Fig. 4*B*, *lanes 4* and *6*), suggesting a dynamic arrangement of the secretin N-terminal domains in the functional secretion system.

DISCUSSION

The similarity in structure of the HR domain of the T2SS and PilP of the T4PS suggests their evolution from a common ancestral domain, which strengthens the evolutionary link between these export machines, a link that did not previously extend to these core proteins of the inner membrane subcomplex. As both domains are located in the periplasm and are associated with machines that assemble pilins either to form a pilus (T4PS) or to push proteins through the outer membrane secretin (T2SS), the structural similarity may extend to a similarity in function. The HR domain binds to the N0 domain of the T2SS secretin and so by analogy, PilP has been shown to interact with the T4PS secretin stabilizing the complex (32).

It is clear from the *in vivo* studies that the interactions within the secretion system are dynamic. Probing the interaction between N0 and N1 of OutD in the functional secretion system confirmed that the interaction surface seen in the crystal complex of the N-terminal periplasmic domains of GspD with nanobody (18), mainly involving strands β3 and β6, corresponds to one of the functional arrangements of these domains *in vivo*, but we also discovered that the N0 domain can interact with a neighboring N0 domain through the same β3 strand. Interestingly, the crystal structure of the N-terminal region of EscC, the secretin from the type III secretion system, showed another mode of mutual arrangement of N0 and N1 domains (19), suggesting the dynamic character of interactions involving N-terminal domains of secretin. The binding of the OutC-HR domain to OutD-N0 must also be dynamic as β3 strand of N0 is

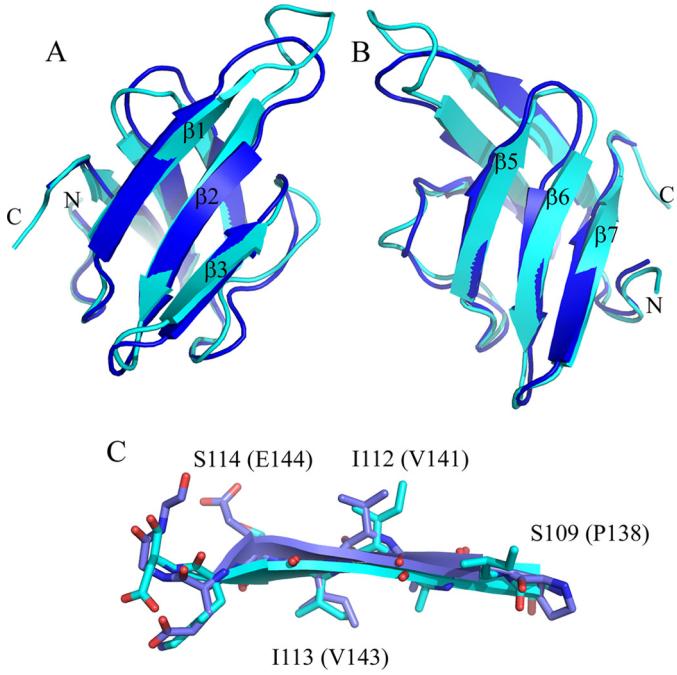

FIGURE 6. **Comparison of the solution structure and the crystal structure of the HR domain.** The solution structure of OutC-HR and crystal structure of GspD-HR are in *cyan* and *blue*, respectively. *A* and *B* are schematic representations looking down on to the first and second β-sheets. *C* illustrates the structural similarity between the structures for a central sheet strand, β2. Residue numbers are for OutC-HR, with those for GspD-HR in parentheses.

also detected in this interaction. When this paper was being published, the crystal structure of the enterotoxigenic *E. coli* GspC-HR·GspD-N0-N1 complex (Protein Data Bank code 3OSS) was described (33). The GspC-HR crystal structure is closely similar to our solution structure of OutC-HR (Fig. 6). The two HR domains have 35% sequence identity, and the 65 equivalent α-carbon atoms superimpose with an r.m.s.d. of 1.3 Å. In the crystal structure β1 of HR interacts with β1 of N0 and not β3 of N0. One explanation for this might be that the β3 region of N0 is particularly sticky and that it prefers to bind N1 but that in the absence of N1, it binds β1 of HR. There is clearly an argument that with both N0 and N1 domains present in the crystal structure, it will be more representative of the situation in the assembled secretion system, but both the solution structure and the crystal structure may be poor mimics of the organization present in the functional secretion system where the dodecameric arrangement of GspD/OutD subunits interacts with a likely hexameric or dodecameric arrangement of GspC/OutC subunits as well as with the other components of the T2SS and secreted proteins.

Our NMR study was initiated because the binding between the soluble regions of OutC and OutD was weak and so co-crystallization was not a possibility. The effectiveness of pulldown assays of OutC with OutD can be improved by co-expression or by partial unfolding in urea followed by refolding, but even then the complex is not stable in size exclusion chromatography even in conditions of low salt (16). The corresponding interaction for the enterotoxigenic *E. coli* GspC/GspD is clearly of higher affinity and can apparently be trapped more easily in the crystal. This apparently points to subtle differences between the secretion systems. Further research is clearly needed to establish the interactions between these and other domains in the context of the assembled secretion system and the way in which these interactions change during the secretion cycle.

In conclusion, this study completes the picture revealing that all core components of the T2SS have a structural ortholog within the T4PS. It also suggests the importance of β1 of the HR domain of the inner membrane subcomplex in interaction with β3 of the N0 domain of the secretin.

REFERENCES

1. Filloux, A. (2004) The underlying mechanisms of type II protein secretion. *Biochim. Biophys. Acta* **1694,** 163–179
2. Cianciotto, N. P. (2005) Type II secretion: A protein secretion system for all seasons. *Trends Microbiol.* **13,** 581–588
3. Chami, M., Guilvout, I., Gregorini, M., Rémigy, H. W., Müller, S. A., Valerio, M., Engel, A., Pugsley, A. P., and Bayan, N. (2005) Structural insights into the secretin PulD and its trypsin-resistant core. *J. Biol. Chem.* **280,** 37732–37741
4. Reichow, S. L., Korotkov, K. V., Hol, W. G., and Gonen, T. (2010) Structure of the cholera toxin secretion channel in its closed state. *Nat. Struct. Mol. Biol.* **17,** 1226–1232
5. Py, B., Loiseau, L., and Barras, F. (2001) An inner membrane platform in the type II secretion machinery of Gram-negative bacteria. *EMBO Rep.* **2,** 244–248
6. Camberg, J. L., Johnson, T. L., Patrick, M., Abendroth, J., Hol, W. G., and Sandkvist, M. (2007) Synergistic stimulation of EpsE ATP hydrolysis by EpsL and acidic phospholipids. *EMBO J.* **26,** 19–27
7. Peabody, C. R., Chung, Y. J., Yen, M. R., Vidal-Ingigliardi, D., Pugsley, A. P., and Saier, M. H. (2003) Type II protein secretion and its relationship to bacterial type IV pili and archaeal flagella. *Microbiology* **149,** 3051–3072
8. Hazes, B., and Frost, L. (2008) Towards a systems biology approach to study type II/IV secretion systems. *Biochim. Biophys. Acta* **1778,** 1839–1850
9. Sampaleanu, L. M., Bonanno, J. B., Ayers, M., Koo, J., Tammam, S., Burley, S. K., Almo, S. C., Burrows, L. L., and Howell, P. L. (2009) Periplasmic domains of *Pseudomonas aeruginosa* PilN and PilO form a stable heterodimeric complex. *J. Mol. Biol.* **394,** 143–159
10. Abendroth, J., Rice, A. E., McLuskey, K., Bagdasarian, M., and Hol, W. G. (2004) The crystal structure of the periplasmic domain of the type II secretion system protein EpsM from *Vibrio cholerae*: The simplest version of the ferredoxin fold. *J. Mol. Biol.* **338,** 585–596
11. Abendroth, J., Kreger, A. C., and Hol, W. G. (2009) The dimer formed by the periplasmic domain of EpsL from the type 2 secretion system of *Vibrio parahaemolyticus*. *J. Struct. Biol.* **168,** 313–322
12. Karuppiah, V., and Derrick, J. P. (2011) Structure of the PilM-PilN inner membrane type IV pilus biogenesis complex from *Thermus thermophilus*. *J. Biol. Chem.* **286,** 24434–24442
13. Login, F. H., and Shevchik, V. E. (2006) The single transmembrane segment drives self-assembly of OutC and the formation of a functional type II secretion system in *Erwinia chrysanthemi*. *J. Biol. Chem.* **281,** 33152–33162
14. Bouley, J., Condemine, G., and Shevchik, V. E. (2001) The PDZ domain of OutC and the N-terminal region of OutD determine the secretion specificity of the type II out pathway of *Erwinia chrysanthemi*. *J. Mol. Biol.* **308,** 205–219
15. Korotkov, K. V., Krumm, B., Bagdasarian, M., and Hol, W. G. (2006) Structural and functional studies of EpsC, a crucial component of the type 2 secretion system from *Vibrio cholerae*. *J. Mol. Biol.* **363,** 311–321
16. Login, F. H., Fries, M., Wang, X., Pickersgill, R. W., and Shevchik, V. E. (2010) A 20-residue peptide of the inner membrane protein OutC mediates interaction with two distinct sites of the outer membrane secretin OutD and is essential for the functional type II secretion system in *Erwinia chrysanthemi*. *Mol. Microbiol.* **76,** 944–955
17. Korotkov, K. V., Gonen, T., and Hol, W. G. (2011) Secretins: Dynamic channels for protein transport across membranes. *Trends Biochem. Sci.* **36,** 433–443

18. Korotkov, K. V., Pardon, E., Steyaert, J., and Hol, W. G. (2009) Crystal structure of the N-terminal domain of the secretin GspD from ETEC determined with the assistance of a nanobody. *Structure* **17,** 255–265
19. Spreter, T., Yip, C. K., Sanowar, S., André, I., Kimbrough, T. G., Vuckovic, M., Pfuetzner, R. A., Deng, W., Yu, A. C., Finlay, B. B., Baker, D., Miller, S. I., and Strynadka, N. C. (2009) A conserved structural motif mediates formation of the periplasmic rings in the type III secretion system. *Nat. Struct. Mol. Biol.* **16,** 468–476
20. Shevchik, V. E., Robert-Baudouy, J., and Condemine, G. (1997) Specific interaction between OutD, an *Erwinia chrysanthemi* outer membrane protein of the general secretory pathway, and secreted proteins. *EMBO J.* **16,** 3007–3016
21. Shen, Y., Lange, O., Delaglio, F., Rossi, P., Aramini, J. M., Liu, G., Eletsky, A., Wu, Y., Singarapu, K. K., Lemak, A., Ignatchenko, A., Arrowsmith, C. H., Szyperski, T., Montelione, G. T., Baker, D., and Bax, A. (2008) Consistent blind protein structure generation from NMR chemical shift data. *Proc. Natl. Acad. Sci. U.S.A.* **105,** 4685–4690
22. Shen, Y., Vernon, R., Baker, D., and Bax, A. (2009) *De novo* protein structure generation from incomplete chemical shift assignments. *J. Biomol. NMR* **43,** 63–78
23. Delaglio, F., Grzesiek, S., Vuister, G. W., Zhu, G., Pfeifer, J., and Bax, A. (1995) NMRPipe: A multidimensional spectral processing system based on UNIX pipes. *J. Biomol. NMR* **6,** 277–293
24. Bartels, C., Xia, T. H., Billeter, M., Guntert, P., and Wuthrich, K. (1995). The program XEASY for computer-supported NMR spectral-analysis of biological macromolecules. *J. Biomol. NMR* **6,** 1–10
25. Fesik, S. W., and Zuiderweg, E. R. (1988) Heteronuclear 3-dimensional NMR spectroscopy–A strategy for the simplification of homonuclear two-dimensional NMR-spectra. *J. Magn. Reson.* **78,** 588–593
26. Shen, Y., and Bax, A. (2007) Protein backbone chemical shifts predicted from searching a database for torsion angle and sequence homology. *J. Biomol. NMR* **38,** 289–302
27. Shen, Y., Delaglio, F., Cornilescu, G., and Bax, A. (2009) TALOS+: A hybrid method for predicting protein backbone torsion angles from NMR chemical shifts. *J. Biomol. NMR* **44,** 213–223
28. Cordier, F., and Grzesiek, S. (1999) Direct observation of hydrogen bonds in proteins by interresidue (3h)J(NC') scalar couplings. *J. Am. Chem. Soc.* **121,** 1601–1602
29. Linge, J. P., Habeck, M., Rieping, W., and Nilges, M. (2003) ARIA: Automated NOE assignment and NMR structure calculation. *Bioinformatics* **19,** 315–316
30. Golovanov, A. P., Balasingham, S., Tzitzilonis, C., Goult, B. T., Lian, L. Y., Homberset, H., Tønjum, T., and Derrick, J. P. (2006) The solution structure of a domain from the *Neisseria meningitidis* lipoprotein PilP reveals a new β-sandwich fold. *J. Mol. Biol.* **364,** 186–195
31. Dominguez, C., Boelens, R., and Bonvin, A. (2003) HADDOCK: A protein-protein docking approach based on biochemical or biophysical information. *J. Am. Chem. Soc.* **125,** 1731–1737
32. Balasingham, S. V., Collins, R. F., Assalkhou, R., Homberset, H., Frye, S. A., Derrick, J. P., and Tønjum, T. (2007) Interactions between the lipoprotein PilP and the secretin PilQ in *Neisseria meningitidis*. *J. Bacteriol.* **189,** 5716–5727
33. Korotkov, K. V., Johnson, T. L., Jobling, M. G., Pruneda, J., Pardon, E., Heroux, A., Turley, S., Steyaert, J., Holmes, R. K., Sandkvist, M., and Hol, W. G. (2011) Structural and functional studies of the interaction of GspC and GspD in the type II secretion system. *PloS Pathog.* **7,** e1002228